

# Slit-Robo signaling induces malignant transformation through Hakai-mediated E-cadherin degradation during colorectal epithelial cell carcinogenesis

Wei-Jie Zhou<sup>1,\*</sup>, Zhen H Geng<sup>2,\*</sup>, Shan Chi<sup>1,\*</sup>, Wenli Zhang<sup>3,\*</sup>, Xiao-Feng Niu<sup>1,\*</sup>, Shu-Jue Lan<sup>1,\*</sup>, Li Ma<sup>2</sup>, Xuesong Yang<sup>4</sup>, Li-Jing Wang<sup>5</sup>, Yan-Qing Ding<sup>3</sup>, Jian-Guo Geng<sup>2,5</sup>

<sup>1</sup>Laboratory of Molecular Cell Biology, Institute of Biochemistry and Cell Biology, Shanghai Institutes for Biological Sciences, Chinese Academy of Sciences, 320 Yue-Yang Road, Shanghai 200031, China; <sup>2</sup>Department of Biologic and Materials Sciences, University of Michigan School of Dentistry, Ann Arbor, MI 48109, USA; <sup>3</sup>Department of Pathology, Nanfang Hospital and School of Basic Medical Sciences, Southern Medical University, Guangzhou, Guangdong 510515, China; <sup>4</sup>Key Laboratory for Regenerative Medicine of the Ministry of Education, Medical College, Jinan University, Guangzhou, Guangdong 510632, China; <sup>5</sup>Vascular Biology Research Institute, Guangdong Pharmaceutical University, Guangzhou, Guangdong 510006, China

**The Slit family of guidance cues binds to Roundabout (Robo) receptors and modulates cell migration. We report here that ectopic expression of Slit2 and Robo1 or recombinant Slit2 treatment of Robo1-expressing colorectal epithelial carcinoma cells recruited an ubiquitin ligase Hakai for E-cadherin (E-cad) ubiquitination and lysosomal degradation, epithelial-mesenchymal transition (EMT), and tumor growth and liver metastasis, which were rescued by knockdown of Hakai. In contrast, knockdown of endogenous Robo1 or specific blockade of Slit2 binding to Robo1 prevented E-cad degradation and reversed EMT, resulting in diminished tumor growth and liver metastasis. Ectopic expression of Robo1 also triggered a malignant transformation in Slit2-positive human embryonic kidney 293 cells. Importantly, the expression of Slit2 and Robo1 was significantly associated with an increased metastatic risk and poorer overall survival in colorectal carcinoma patients. We conclude that engagement of Robo1 by Slit2 induces malignant transformation through Hakai-mediated E-cad ubiquitination and lysosomal degradation during colorectal epithelial cell carcinogenesis.**

**Keywords:** colorectal carcinogenesis; E-cadherin; Hakai; Robo; Slit

*Cell Research* (2011) 21:609-626. doi:10.1038/cr.2011.17; published online 1 February 2011

## Introduction

The Slit family of guidance cues interacts with the Roundabout (Robo) family of transmembrane receptors in a wide variety of physiological processes requiring cell migration [1-4]. Slit-Robo signaling regulates the repulsion or attraction of projecting axons, and migrating neurons during development of the nervous system [5, 6]. Slit2 secreted by vascular endothelial cells binds to

Robo1 on leukocytes and acts as an endogenous inhibitor of leukocyte chemotaxis [7-12]. Additionally, Slit2 mediates directional migration of malignant cells [13-15]. We and others have previously reported that Slit proteins secreted by solid tumors binds to Robo1 expressed on vascular and lymphatic endothelial cells to stimulate angiogenesis and lymphangiogenesis [16-22]. Although such paracrine pathways involving Slit-Robo interactions have been extensively studied, the biological significance and molecular mechanisms of autocrine Slit-Robo signaling are largely unexplored.

E-cadherin (E-cad) functions as a cell adhesion molecule in adherens junction [23-26]. The cytoplasmic region of E-cad directly interacts with  $\beta$ -catenin ( $\beta$ -cat), which in turn interacts with  $\alpha$ -catenin ( $\alpha$ -cat) and other molecules to link it to the actin cytoskeleton [27]. Loss

\*These six authors contributed equally to this work.

Correspondence: Jian-Guo Geng<sup>a</sup>, Yan-Qing Ding<sup>b</sup>

<sup>a</sup>E-mail: genglab@gmail.com

<sup>b</sup>E-mail: dyqsmu@sina.com

Received 9 September 2010; revised 19 September 2010; accepted 21 September 2010; published online 1 February 2011

of E-cad leads to cell-cell dissociation and acquisition of a migratory phenotype during development, tissue remodeling or carcinogenesis [28-35]. In addition to E-cad, other molecular constituents of the adherens junction have important roles in maintaining cell-cell adhesion within the epithelium and preventing tumor invasiveness during carcinogenesis. Among them,  $\alpha$ -cat is essential for coordinating actin dynamics and inversely linking cell adhesion with proliferation [36].

We have previously reported elevated expression of Slit2 in human colorectal carcinoma tissues and cell lines [16]. Using cDNA microarray, a significant upregulation of Robo1 was found in colorectal carcinoma tissues [37]. Overexpression of Robo1 is also detected in transforming growth factor (TGF)- $\beta$  and Wnt-induced intestinal tumors [38]. Taken together, these results suggest the possibility of an autocrine mechanism through which colorectal carcinoma cells secrete Slit2 for signaling through Robo1 expressed on these same cells. This study investigated the biological significance and the molecular mechanism of autocrine Slit-Robo signaling in recruitment of Hakai, ubiquitination and lysosomal degradation of E-cad, cumulating to induction of epithelial-mesenchymal transition (EMT) and malignant transformation during the pathogenesis of colorectal epithelial cell carcinoma. Various *in vitro* assays, *in vivo* animal models, and analysis of patient samples were used to evaluate the effects of Slit2-Robo1 interaction on carcinogenesis of colorectal epithelial cells.

## Results

### *Expression of Slit2 and Robo1 in human colorectal carcinoma cells*

We examined the expression of Slit2 and Robo1 in 10 human colorectal carcinoma cell lines using Slit2 and Robo1 monoclonal antibodies (mAbs) [16]. Elevated Slit2 secretion or Robo1 and Slit2 expression (~180 kDa for Slit2 and ~200 kDa for Robo1) was seen in the supernatants and lysates of six cell lines: SW620, SW480, LS180, LS174T, Lovo and Caco2 cells (Figure 1A). However, neither Robo1 nor Slit2 secretion/expression was evident in the other four cell lines; SW48, HCT116, HT29 and DLD1 cells. Human embryonic kidney 293 (HEK293) cells stably overexpressing Slit2 or Robo1 [16] were used as positive controls.  $\alpha$ -Tubulin (~55 kDa) was used in parallel as a sample loading control. The protein expression profile for each cell line was consistent with its mRNA levels for Robo1-4 and Slit1-3, as determined by quantitative real-time reverse transcription-polymerase chain reaction (qRT-PCR; Supplementary information, Data S1 and Figure S1A). Robo4 mRNA was not

detected in any of the cell lines, even though it was clearly present in human umbilical vein endothelial cells (data not shown). Notably, Slit2 secretion or Slit2 and Robo1 expression was higher in metastatic SW620 cells than SW480 cells isolated from primary tumor (Supplementary information, Figure S1B), suggesting that secreted Slit2 may bind to cell-surface Robo1 to initiate Slit2-Robo1 signaling in colorectal carcinoma cells.

### *Slit-Robo signaling triggers a fibroblast-like morphology*

E-cad is required for normal epithelial cell morphology and formation of cell-cell adherens junctions in the epithelial monolayer [23-26]. We, thus, speculated whether Slit-Robo signaling may alter cell morphology through downregulation of E-cad and other epithelial cell markers. To test this hypothesis, we performed gain- or loss-of-function studies in HCT116 cells lacking detectable Slit2 and Robo1 expression and SW620 cells overexpressing endogenous Slit2 and Robo1 (Figure 1A). Compared with HCT116 cells stably transfected with plain vector (HCT116/V), HCT116 cells stably transfected with Robo1 (HCT116/Robo1), Slit2 (HCT116/Slit2) or Slit2 plus Robo1 (HCT116/Robo1/Slit2) exhibited increased expression of their respective transgene products (Figure 1B, left panel and data not shown). Compared with SW620 cells stably transfected with plain vector (SW620/V), stable knockdown of Robo1 RNA by short hairpin RNA (shRNA) technology in SW620 cells (SW620/shRobo1) resulted in decreased levels of Robo1 protein (Figure 1B, right panel). Notably, we previously generated R5, a mAb that recognizes the first immunoglobulin-like domain of human, rat and mouse Robo1, and neutralizes Slit2 binding [16]. Using isolated recombinant human Slit2 (hSlit2) and recombinant human Robo1-Fc (hRobo1-Fc; Supplementary information, Figure S2A), we found that R5, but not isotype-matched irrelevant mouse immunoglobulin G (mIgG), inhibited the binding of human Robo1-Fc to immobilized hSlit2 (Supplementary information, Data S1 and Figure S2B). These data confirmed that R5 acts as a neutralizing mAb to Robo1 that prevents Slit2 recognition. We extensively used hSlit2 to mimic autocrine Slit2-Robo1 signaling for stimulation of Robo1-expressing cells or R5 to block the binding of endogenous Slit2 to Robo1 in the experiments.

Surprisingly, HCT116/Robo1/Slit2 cells developed elongated and spindle-shaped morphology that resembled fibroblast-like mesenchymal cells, whereas no such change in morphology was observed in HCT116/V, HCT116/Robo1 or HCT116/Slit2 cells (Figure 1C, upper panel and data not shown). Following knockdown of Robo1, SW620/shRobo1 cells developed a round cobble-

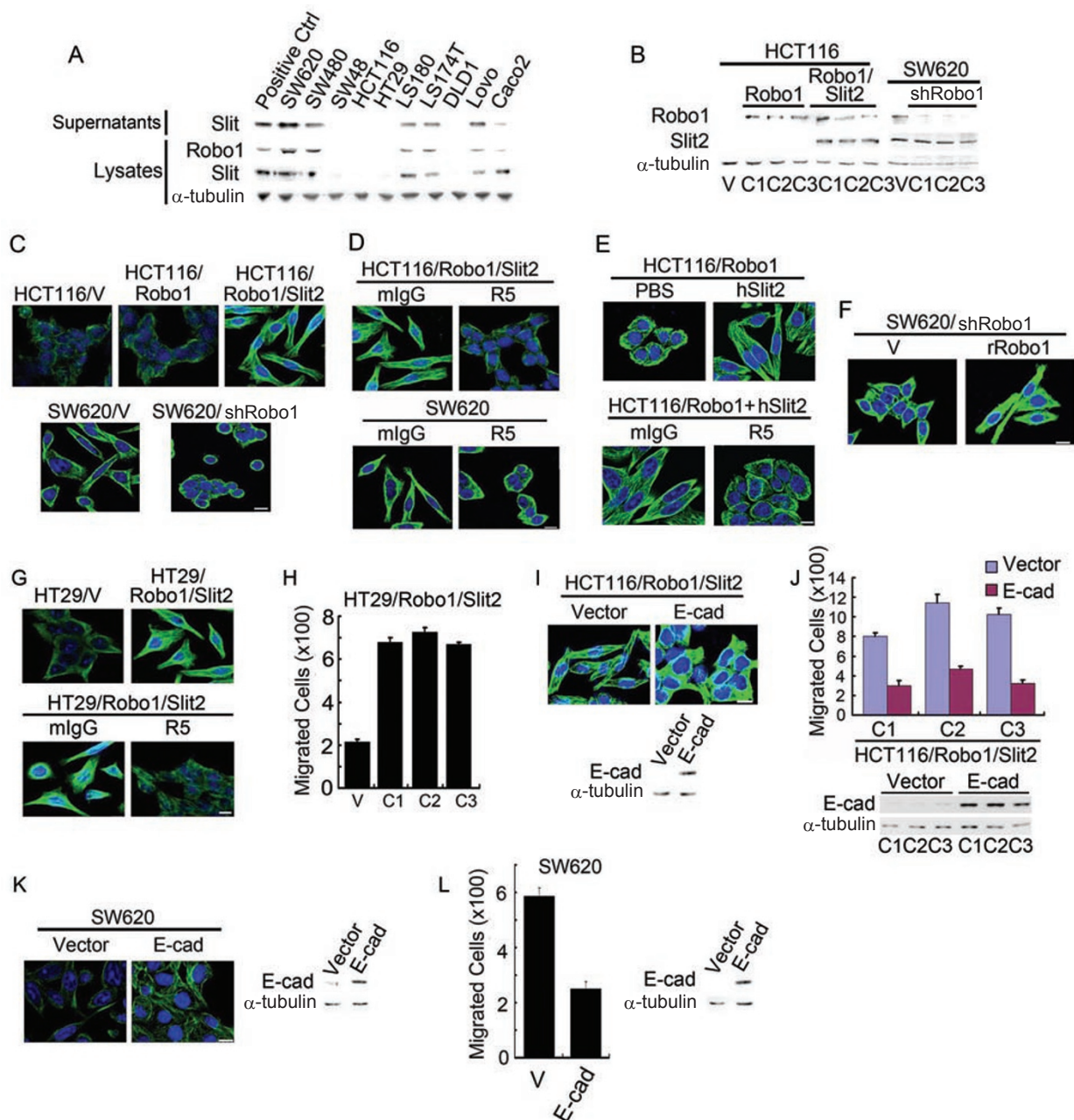


**Figure 1** Slit-Robo signaling elicits fibroblast-like morphology. **(A)** Slit2 and Robo1 expression in human colorectal carcinoma cell lines detected by immunoblotting analysis with mAbs to Robo1, Slit2 and  $\alpha$ -tubulin. **(B)** HCT116 cells stably transfected with plain vector (HCT116/V) or plasmid encoding Robo1 (HCT116/Robo1) or Robo1 plus Slit2 (HCT116/Robo1/Slit2) and SW620 cells stably transfected with plain vector (SW620/V) or plasmid encoding shRNA for Robo1 knockdown (SW620/shRobo1). Detergent lysates were immunoblotted with the Robo1, Slit2 and  $\alpha$ -tubulin mAbs. C1-3, single cell clones 1-3. **(C-F)** Morphological features of HCT116/V, HCT116/Robo1 (C1), HCT116/Robo1/Slit2 (C1), SW620/V and SW620/shRobo1 (C1) cells in the absence and presence of mlgG, R5, PBS and hSlit2 **(C-E)** or transfected with the plain vector or the plasmid of rat Robo1 **(F)**. They were immunofluorescently stained for  $\alpha$ -tubulin (green) and nuclear DNAs with DAPI (blue). **(G-L)** Morphologic and migratory features of HT29/V and HT29/Robo1/Slit2 cells, HCT116/Robo1/Slit2 cells or SW620 cells transfected with the plain vector or the plasmid of E-cad in the absence and presence of mlgG or R5. Cell migratory activities were determined using the Boyden chamber assay as described previously [16]. Lysates were also immunoblotted for E-cad and  $\alpha$ -tubulin. Bars, 10  $\mu$ m. Results are representative of at least three separate experiments **(A-G, I and K)** or the mean  $\pm$  S.D. of three independent experiments **(H, J and L)**.

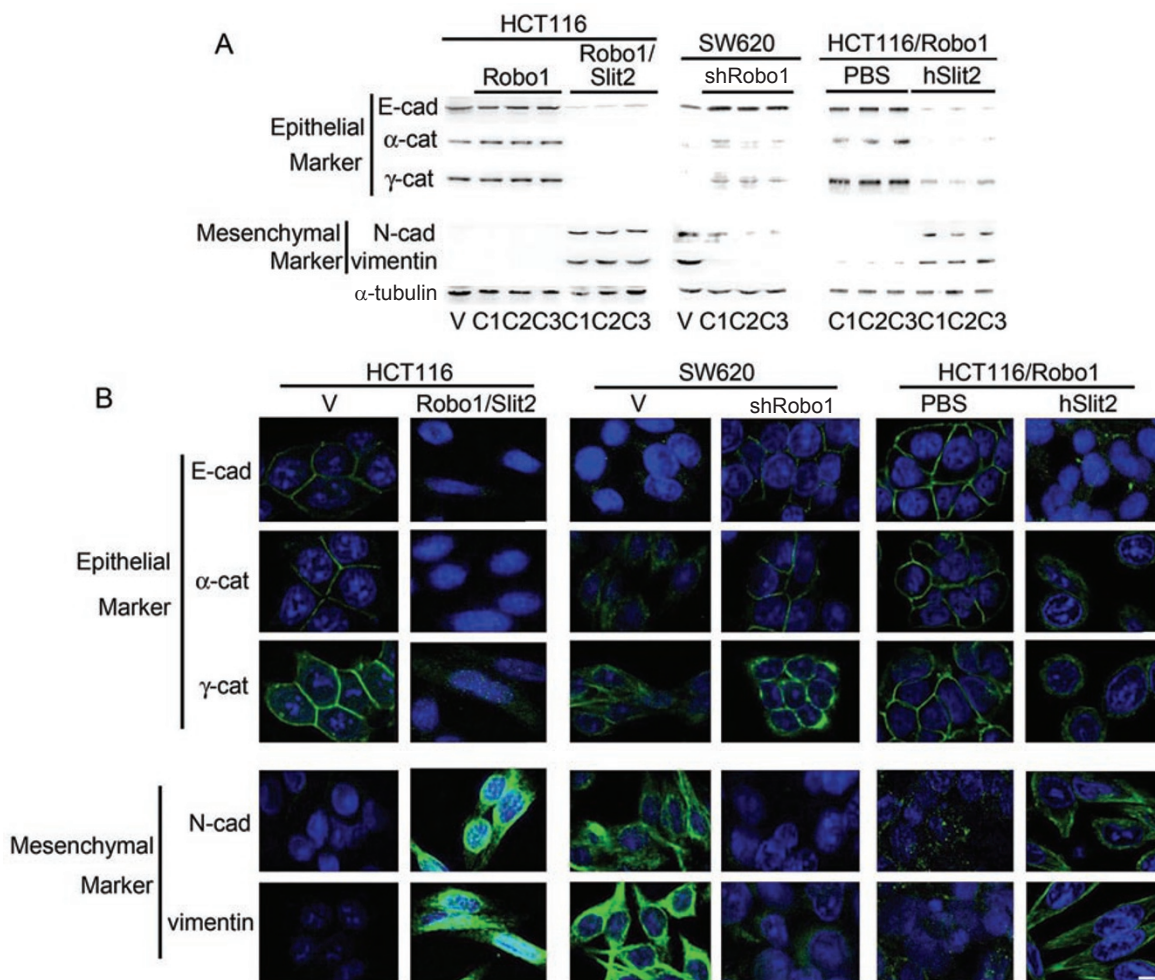


**Figure 2** Slit-Robo signaling elicits mesenchymal markers. Expression of epithelial markers and mesenchymal markers in HCT116/V, HCT116/Robo1, HCT116/Robo1/Slit2, SW620/V and SW620/shRobo1 cells in the absence and presence of PBS and hSlit2. They were detected by immunoblotting (A) and immunofluorescent staining (B). HCT116/Robo1 (C1), HCT116/Robo1/Slit2 (C1) and SW620/shRobo1 (C1) cells were used for immunofluorescent staining as above. Bars, 10  $\mu$ m. Results are representative of at least three independent experiments.

stone shape similar in morphology to epithelial cells (Figure 1C, lower panel). Analogously, HCT116/Robo1/Slit2 cells (Figure 1D, upper panel) and SW620 cells (Figure 1D, lower panel) acquired an epithelial cell-like phenotype when they were treated with R5, but not with mIgG. Incubation with hSlit2 switched HCT116/Robo1 cells from an epithelial-like morphology to a mesenchymal-like morphology (Figure 1E, upper panel), which was neutralized by R5, but not by mIgG (Figure 1E, lower panel), attesting to the functional significance of Slit2 in induction of fibroblast-like morphology for colorectal epithelial cells. Following transfection with the plasmid of rat Robo1 (rRobo1) or the plain vector (V), we found that only rRobo1-reintroduced SW620/shRobo1 cells back to a mesenchymal-like morphology (Figure 1F),

thus eliminating the possibility of an off-target effect for the Robo1 shRNA plasmid used.

In support of our findings, we found that in analogous to HCT116 cells, HT29 cells lacked expression of Slit2 and Robo1 (Figure 1A). However, stable overexpression of Robo1 and Slit2 in HT29 (HT29/Robo1/Slit2) cells also induced a fibroblast-like morphology with long, slender processes compared with HT29 cells transfected with the plain vector (HT29/V), which was reversed by treatment with R5, but not with mIgG (Figure 1G). Compared with the plain vector, ectopic expression of E-cad (Figure 1I, lower panel and Figure 1K, right panel) switched the mesenchymal-like morphology back to the epithelial-like morphology in HCT116/Robo1/Slit2 cells (Figure 1I, upper panel) and SW620 cells (Figure

1K, left panel), further demonstrating the importance of Slit-Robo signaling-induced E-cad modulation in maintenance of epithelial-like features in the morphology of colorectal epithelial cells.

#### *Slit-Robo signaling induces EMT markers*

We next assessed whether Slit2-Robo1 signaling modulates cell morphology in a way indicative of EMT in colorectal carcinoma cells. Compared with HCT116/V cells and HCT116/Robo1 cells, HCT116/Robo1/Slit2 cells displayed dramatically decreased expression of the epithelial markers E-cad (~120 kDa),  $\alpha$ -cat (~102 kDa) and  $\gamma$ -cat (~82 kDa), along with significantly increased expression of the mesenchymal markers N-cad (~120 kDa) and vimentin (~58 kDa; Figure 2A and 2B, left panels). In contrast, SW620/shRobo1 cells showed the opposite profile of these molecular markers, with evidence of augmented expression of E-cad,  $\alpha$ -cat and  $\gamma$ -cat and reduced the expression of N-cad and vimentin, as compared with SW620/V cells (Figure 2A and 2B, middle panels). Furthermore, incubation of HCT116/Robo1 cells with hSlit2, but not phosphate-buffered saline (PBS), downregulated E-cad,  $\alpha$ -cat and  $\gamma$ -cat while upregulating N-cad and vimentin (Figure 2A and 2B, right panels). On the basis of these findings, it is reasonable to surmise that Slit2-Robo1 signaling modulates the expression of E-cad and other EMT markers to reversibly control the transition between epithelial and mesenchymal phenotypes.

#### *Slit-Robo signaling enhances tumor growth and liver metastasis*

Given that Slit-Robo signaling induces EMT in colorectal carcinoma cells, we examined whether Slit-Robo signaling promotes cell transformation by increasing cell proliferation and migration, and thereby enhancing tumor growth and metastasis. Compared with HCT116/V cells, HCT116/Robo1/Slit2 cells grew faster (Figure 3A), migrated more rapidly (Figure 3B), and formed more colonies (Figure 3C) *in vitro*. When inoculated subcutaneously into athymus nude mice, HCT116/Robo1/Slit2 cells grew faster (Figure 3D) and metastasized to the liver (Figure 3E) *in vivo*. In contrast, SW620/shRobo1 cells grew more slowly (Figure 3F), migrated less rapidly (Figure 3G) and formed fewer colonies (Figure 3H) *in vitro* compared with SW620/V cells. Mice inoculated subcutaneously with SW620/shRobo1 cells had dramatically reduced tumor volumes (Figure 3I) and no liver metastasis (Figure 3J). Treatment of HCT116/Robo1/Slit2 and SW620 cells with R5, but not with mIgG, also inhibited *in vitro* proliferation (Figure 3K and 3L), migration (Figure 3M) and colony formation (Figure 3N). In mice inoculated subcutaneously with HCT116/Robo1/

Slit2 cells or SW620 cells, R5, but not mIgG, attenuated *in vivo* tumor growth (Figure 3O and 3P) and metastasis (Figure 3Q). Similarly, HT29/Robo1/Slit2 cells manifested enhanced migration compared with HT29/V cells (Figure 1H), which was inhibited by R5, but not by mIgG (data not shown). Overexpression of E-cad (Figure 1J, lower panel and Figure 1L, right panel) reduced the ability of HCT116/Robo1/Slit2 cells (Figure 1J, upper panel) and SW620 cells (Figure 1L, left panel) to migrate through the membranes of Boyden chamber. As the matter of fact, it was quite amazing to us to find that ectopic expression of Slit2 and Robo1 markedly accelerated HCT116 cell growth (Figure 3D, right panel), while knockdown of Robo1 almost abolished SW620 cell growth (Figure 3I, right panel) in the murine xenograft model. Taken together, these *in vitro* and *in vivo* results demonstrate that Slit-Robo signaling potently promotes tumor growth and metastasis by drastically increasing growth, migration and transformation of colorectal epithelial cells.

#### *Slit-Robo signaling recruits Hakai and ubiquitinates E-cad for lysosomal localization*

Hakai is an E3 ubiquitin ligase that is known to mediate E-cad ubiquitination and lysosomal degradation [31, 39]. We thus investigated whether Slit-Robo signaling might recruit Hakai to E-cad. Compared with HCT116/V and HCT116/Robo1 cells, ectopic expression of Slit2 and Robo1 enhanced the association of E-cad with Hakai in HCT116/Robo1/Slit2 cells, as detected by the anti-Hakai Ab from Santa Cruz Biotechnology (Figure 4A, left panel; ~60 kDa). The E-cad-Hakai association in HCT116/Robo1/Slit2 cells was inhibited by R5, but not by mIgG (Figure 4C, left panel). The E-cad-Hakai association in SW620 cells was also blocked by knockdown of Robo1 mRNA (Figure 4B, left panel) or treatment with R5 (Figure 4C, left panel). In contrast, incubation of HCT116/Robo1 cells with hSlit2, but not PBS, pH 7.4, increased Hakai binding to E-cad, which was neutralized by R5, but not by mIgG (Figure 4D, left panel). Cell lysates were also directly immunoblotted as sample loading controls (Figure 4A-4D, right panels). Notably, the identical results were obtained using another anti-Hakai Ab from Abcam (Supplementary information, Figure S3A-S3D).

Consistent with the recruitment of Hakai, HCT116/Robo1/Slit2 cells manifested a significantly elevated level of E-cad ubiquitination as compared with HCT116/V and HCT116/Robo1 cells (Figure 4E, upper panel). Conversely, SW620/shRobo1 cells displayed markedly diminished E-cad ubiquitination as compared with SW620/V cells (Figure 4F, upper panels). R5, but not mIgG, reduced E-cad ubiquitination in both HCT116/

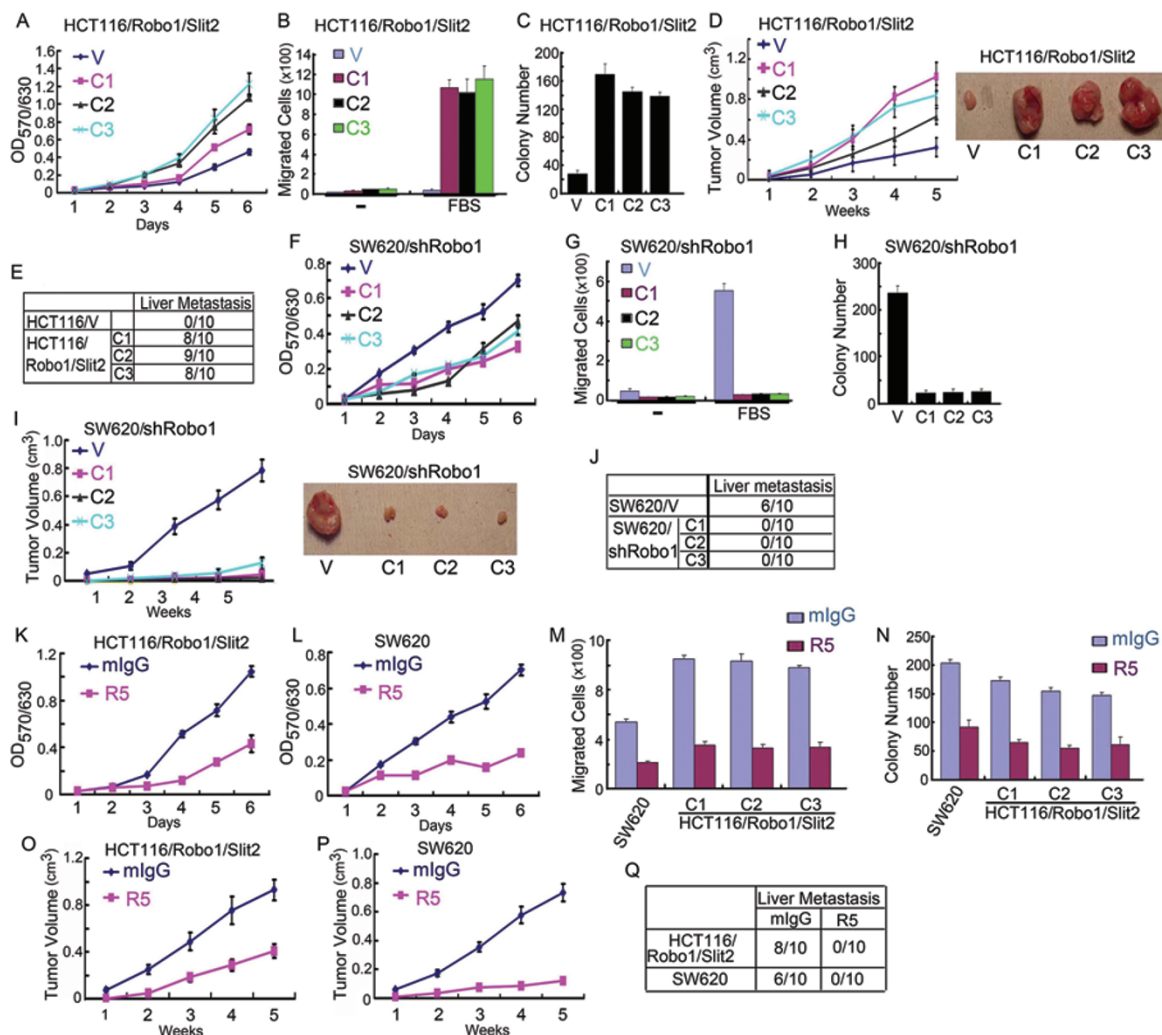


**Figure 3** Slit-Robo signaling promotes intestinal epithelial cell carcinogenesis. (A, F, K and L) *In vitro* growth of HCT116/V and HCT116/Robo1/Slit2 cells (A), SW620/V and SW620/shRobo1 cells (F), HCT116/Robo1/Slit2 cells in the presence of mlgG or R5 (K) and SW620 cells in the presence of mlgG or R5 (L). Cell proliferation activities were measured as before [16]. (B, G and M) Migratory activity of HCT116/V and HCT116/Robo1/Slit2 cells (B), SW620/V and SW620/shRobo1 cells (G) or SW620 and HCT116/Robo1/Slit2 cells in the presence of mlgG or R5 (M). Cell migratory activities were determined using the Boyden chamber assay [16]. (C, H and N) Colony formation of HCT116/V and HCT116/Robo1/Slit2 cells (C), SW620/V and SW620/shRobo1 cells (H) or SW620 and HCT116/Robo1/Slit2 cells in the presence of mlgG or R5 (N). Cell transformation activities were measured by the colony formation assay. (D, I, O and P) Average tumor volume in athymus nude mice subcutaneously inoculated with HCT116/V and HCT116/Robo1/Slit2 cells (D, left panel), SW620/V and SW620/shRobo1 cells (I, left panel) and HCT116/Robo1/Slit2 cells in the presence of mlgG or R5 (O) and SW620 cells in the presence of mlgG or R5 (P). Representative tumor mass of HCT116/V and HCT116/Robo1/Slit2 cells (D, right panel) and SW620/V and SW620/shRobo1 cells (I, right panel). (E, J and Q) Incidence of liver metastasis in athymus nude mice subcutaneously inoculated with HCT116/V and HCT116/Robo1/Slit2 cells (E), SW620/V and SW620/shRobo1 cells (J), and HCT116/Robo1/Slit2 and SW620 cells (Q) in the presence of mlgG or R5. Results represent the mean±S.D. of three independent experiments (A and C, F and H, K and N) or 10 animals for each group (D, I, O and P).

Robo1/Slit2 and SW620 cells (Figure 4G, upper panels). In comparison, incubation of HCT116/Robo1 cells with hSlit2, but not with PBS, augmented E-cad ubiquitination, which was abolished by R5, but not by mlgG (Figure 4H, upper panel). Immunoprecipitated E-cad was also

immunoblotted for E-cad (Figure 4E-4H, lower panels). Our findings, thus, indicate that Slit-Robo signaling increases Hakai binding to E-cad, resulting in E-cad ubiquitination in colorectal epithelial cells.

We next examined whether Slit2 binding to Robo1 enhanced E-cad localization in the lysosome. Using immunofluorescent staining of E-cad and LAMP-1, a lysosome marker, we found that E-cad was indeed localized exclusively on the cell-surface plasma membrane in HCT116/V cells (Figure 5A). In HCT116/Robo1/Slit2 cells, however, E-cad was re-distributed from the cell-surface plasma membrane to the cytoplasm, where it was partially co-localized with LAMP-1. Importantly, R5, but not mIgG, restored the cell-surface localization of E-cad in HCT116/Robo1/Slit2 cells. In SW620 cells, Robo1 knockdown or R5 treatment resulted in the cell-surface localization of E-cad, in contrast to the cytoplasmic and lysosomal localization in untreated SW620/V cells (Figure 5B). Incubation of HCT116/Robo1 cells with hSlit2, but not PBS, also re-distributed E-cad from the cell-surface to the cytoplasmic and lysosomal compartments, which was prevented by R5, but not by mIgG (Figure 5C). Taken together, our results indicate that engagement of Robo1 by Slit2 targets E-cad to the lysosome through E-cad ubiquitination in colorectal epithelial cells.

#### Slit-Robo signaling degrades E-cad through Hakai

Given that Slit-Robo signaling increases E-cad ubiquitination and lysosomal localization, we next tested whether Slit-Robo signaling induces E-cad degradation by measuring the levels of E-cad following inhibition of protein synthesis. Cycloheximide (CHX), an inhibitor of protein synthesis, was incubated with cells for 0, 6 and 12 h. As suspected, E-cad degradation was observed in HCT116/Robo1/Slit2 cells, but not in HCT116/V or HCT116/Robo1 cells (Figure 6A). In contrast, E-cad was protected from degradation in SW620/shRobo1 cells as compared with SW620/V cells (Figure 6B). Incubation of HCT116/Robo1 cells with hSlit2, but not with PBS, also elicited E-cad degradation (Figure 6C). R5, but not mIgG, prevented E-cad degradation in HCT116/Robo1/Slit2 cells (Figure 6D), SW620 cells (Figure 6E) and HCT116/Robo1 cells in the presence of hSlit2 (Figure 6F). In contrast, E-cad degradation was prevented in cells with active Slit2-Robo1 signaling using chloroquin (an inhibitor for lysosomal degradation), MG132 (an inhibitor for proteasomal degradation) or chloroquin plus MG132 (Supplementary information, Figure S4A-S4C, upper panels). Notably, overexpression of Robo1 and Robo1 plus Slit2 in HCT116 cells, Robo1 knockdown in SW620 cells, or hSlit2 incubation of HCT116/Robo1, in the absence or presence of mIgG and R5, had no detect-

uitation and lysosomal localization, we next tested whether Slit-Robo signaling induces E-cad degradation by measuring the levels of E-cad following inhibition of protein synthesis. Cycloheximide (CHX), an inhibitor of protein synthesis, was incubated with cells for 0, 6 and 12 h. As suspected, E-cad degradation was observed in HCT116/Robo1/Slit2 cells, but not in HCT116/V or HCT116/Robo1 cells (Figure 6A). In contrast, E-cad was protected from degradation in SW620/shRobo1 cells as compared with SW620/V cells (Figure 6B). Incubation of HCT116/Robo1 cells with hSlit2, but not with PBS, also elicited E-cad degradation (Figure 6C). R5, but not mIgG, prevented E-cad degradation in HCT116/Robo1/Slit2 cells (Figure 6D), SW620 cells (Figure 6E) and HCT116/Robo1 cells in the presence of hSlit2 (Figure 6F). In contrast, E-cad degradation was prevented in cells with active Slit2-Robo1 signaling using chloroquin (an inhibitor for lysosomal degradation), MG132 (an inhibitor for proteasomal degradation) or chloroquin plus MG132 (Supplementary information, Figure S4A-S4C, upper panels). Notably, overexpression of Robo1 and Robo1 plus Slit2 in HCT116 cells, Robo1 knockdown in SW620 cells, or hSlit2 incubation of HCT116/Robo1, in the absence or presence of mIgG and R5, had no detect-

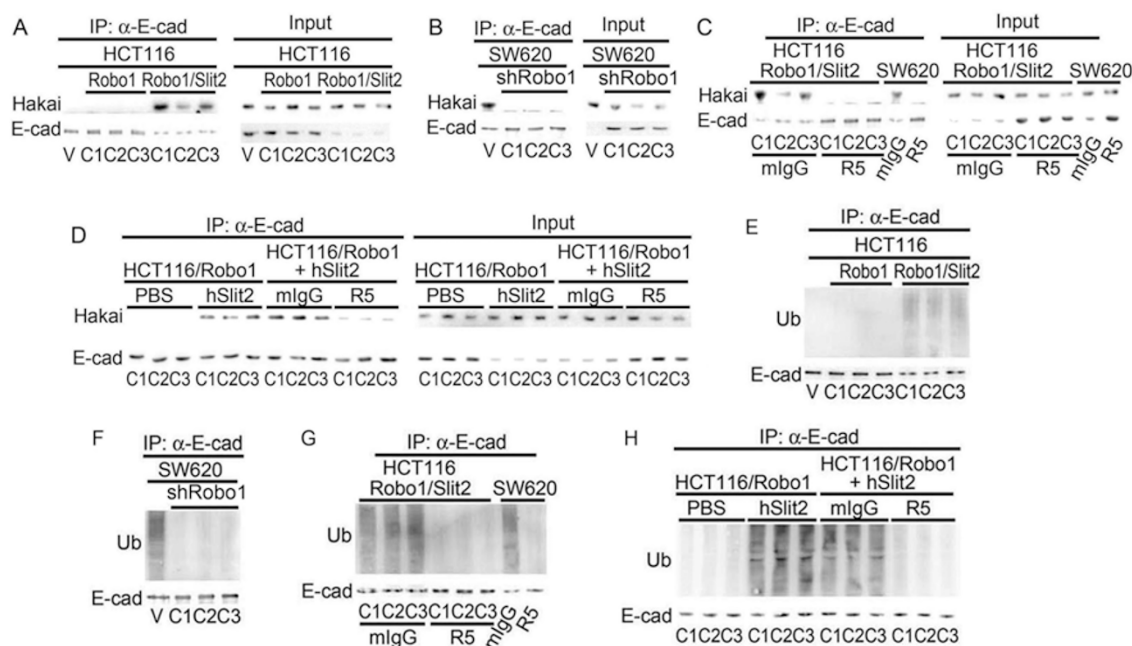


**Figure 4** Slit-Robo signaling recruits Hakai to E-cad and induces E-cad ubiquitination. **(A-D)** Hakai binding to E-cad in HCT116/V, HCT116/Robo1, HCT116/Robo1/Slit2, SW620/V and SW620/shRobo1 cells in the absence or presence of mIgG, R5, PBS and hSlit2. E-cad was immunoprecipitated from the cell lysates followed by immunoblotting with the Abs to E-cad and Hakai. **(E-H)** E-cad ubiquitination in HCT116/V, HCT116/Robo1, HCT116/Robo1/Slit2, SW620/V and SW620/shRobo1 cells in the absence or presence of mIgG, R5, PBS and hSlit2. E-cad was immunoprecipitated from the cell lysates followed by immunoblotting with the ubiquitin and E-cad Abs. Ub, ubiquitin. Results are representative of at least three independent experiments.

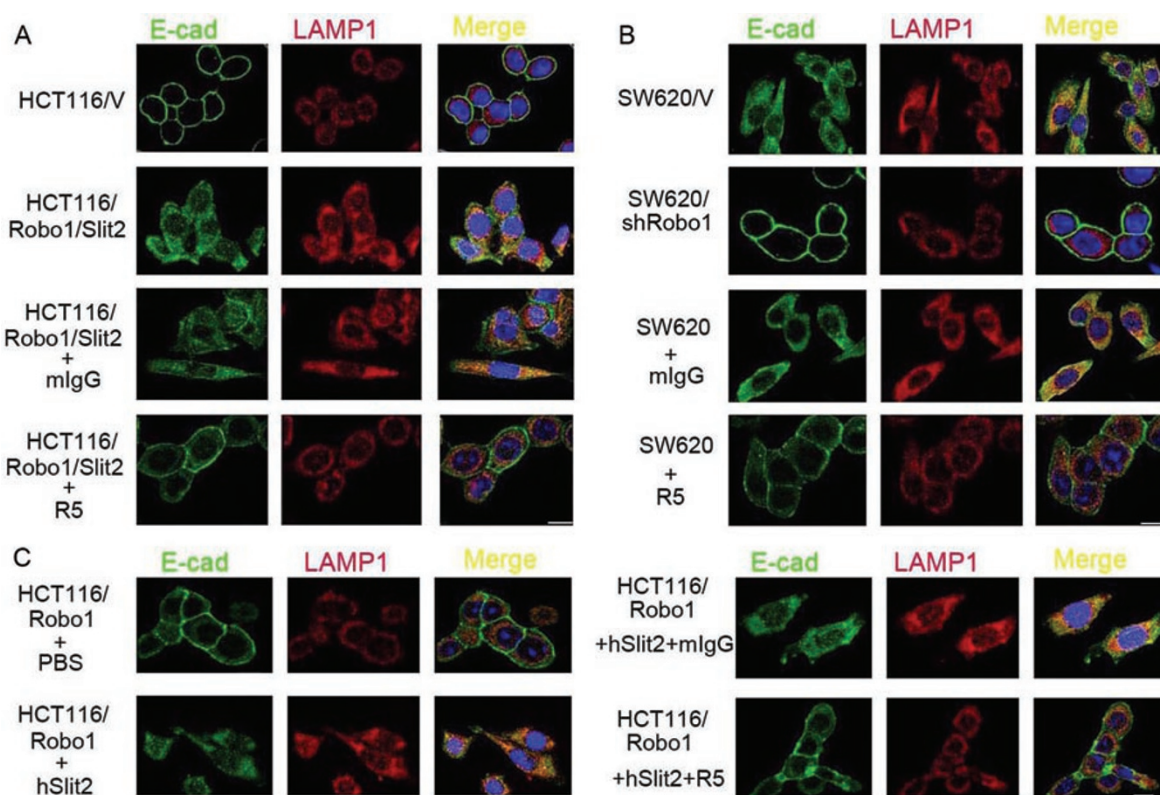


**Figure 5** Slit-Robo signaling triggers E-cad lysosomal localization. **(A)** E-cad and LAMP-1 co-localization in HCT116/V and HCT116/Robo1/Slit2 (C1) cells in the absence or presence of mlgG or R5. Endogenous E-cad and LAMP-1 were immunofluorescent stained with their respective Abs. **(B)** E-cad and LAMP-1 co-localization in SW620/V and SW620/shRobo1 (C1) cells in the absence or presence of mlgG or R5. **(C)** E-cad and LAMP-1 co-localization in HCT116/Robo1 (C1) cells in the absence or presence of PBS, hSlit2, mlgG and R5. Bars, 10  $\mu$ m. Results are representative of at least three independent experiments.

able effects on  $\beta$ -cat degradation (Supplementary information, Figure S4D, upper panels) and ubiquitination (Supplementary information, Figure S4E, upper panels).  $\alpha$ -Tubulin in the cell lysates (Supplementary information, Figure S4A-S4D, lower panels) and the immunoprecipitated  $\beta$ -cat (Supplementary information, Figure S4E, lower panels) were also immunoblotted for sample loading controls.

We next tested whether knockdown of endogenous Hakai could preserve E-cad from its ubiquitination and degradation induced by Slit-Robo signaling. Compared with the shRNA control, Hakai shRNA1 and 2 both potently inhibited Hakai expression (> 95%) in SW620 cells (Figure 7A, upper panel). As predicted, Hakai shRNA1 and 2, but not the shRNA control, drastically reduced E-cad ubiquitination immunoprecipitated from the lysates of HCT116/Robo1/Slit2 cells (Figure 7B, left upper panel), SW620 cells (Figure 7B, right upper panel) and hSlit2-treated HCT116/Robo1 cells (Figure 7C, upper panel). Compared with the shRNA control, Hakai

shRNA1 and 2 markedly reduced E-cad degradation in HCT116/Robo1/Slit2 cells (Figure 7D, upper left panel), SW620 cells (Figure 7D, upper right panel) and hSlit2-incubated HCT116/Robo1 cells (Figure 7E, upper panel). In parallel, immunoprecipitated E-cad (Figure 7B and 7C, middle panels), endogenous Hakai (Figure 7B and 7C, lower panels and Figure 7D and 7E, middle panels) and  $\alpha$ -tubulin (Figure 7D and 7E, lower panels) were immunoblotted with their respective Abs. Consistently, Hakai shRNA1 and 2, but not the shRNA control, avidly switched HCT116/Robo1/Slit2 cells (Figure 7F), SW620 cells (Figure 7G) and hSlit2-incubated HCT116/Robo1 cells (Figure 7H) from the fibroblast-like morphology back to the epithelial-like morphology, with concomitant reduction of their cell migrations (Figure 7I). These results collectively demonstrate the significance of Hakai in mediating E-cad ubiquitination and degradation triggered by Slit-Robo signaling during colorectal epithelial cell carcinogenesis.

### Slit-Robo signaling fails to suppress E-cad transcription

We next explored whether Slit-Robo signaling might reduce E-cad protein levels through transcriptional repression. Using the HCT116 and SW620 cellular models, we examined whether Slit2 binding to Robo1 decreases the transcription of E-cad or increases its known transcriptional repressors. We co-transfected cells with an E-cad promoter luciferase reporter construct and a plasmid encoding a gene of interest or plain vector (V) (Supplementary information, Data S1). The snail plasmid was used as a positive control because it is known to transcriptionally downregulate E-cad [34]. HCT116/V, HCT116/Robo1 and HCT116/Robo1/Slit2 cells failed to appreciably suppress E-cad promoter activity compared with HCT116 cells transfected with the snail plasmid (Supplementary information, Figure S5A). As measured by qRT-PCR, HCT116/Robo1/Slit2 cells exhibited no significant decrease in the mRNA levels of E-cad or increase its transcriptional repressors Twist, Snail, Slug or Zeb2 compared with the mRNA levels in HCT116/V cells (Supplementary information, Figure S5B). In addition, SW620/shRobo1 cells exhibited no obvious increase in mRNA levels of E-cad, Twist, Slug or Zeb2 compared with SW620/V cells (Supplementary informa-

tion, Figure S5C). These data suggest that Slit-Robo signaling does not significantly reduce the levels of E-cad protein through transcriptional suppression of E-cad or its known transcriptional repressors.

### Slit-Robo signaling induces transformation of HEK293 cells

To investigate whether Slit-Robo signaling can also induce transformation in epithelial cells other than colorectal epithelial cells, we established HEK293 cells stably overexpressing Robo1 or plain vector (293/Robo1 and 293/V). Notably, 293/Robo1 cells expressed a considerably high level of endogenous Slit2 (Figure 8A). Interestingly, 293/Robo1 cells manifested a remarkable fibroblast-like phenotype as shown by phase-contrast microscopy and immunofluorescent staining of  $\alpha$ -tubulin and  $\beta$ -actin (Figure 8B) with concomitant downregulation of E-cad,  $\alpha$ -cat and  $\gamma$ -cat in parallel to upregulation of N-cad and vimentin (Figure 8C).  $\alpha$ -Tubulin was immunoblotted in parallel as a sample loading control. Importantly, 293/Robo1 cells grew faster (Figure 8D) and migrated more rapidly (Figure 8E) *in vitro* and formed larger tumors (Figure 8F) following subcutaneous inoculation *in vivo*. These results indicate that Slit-Robo sig-

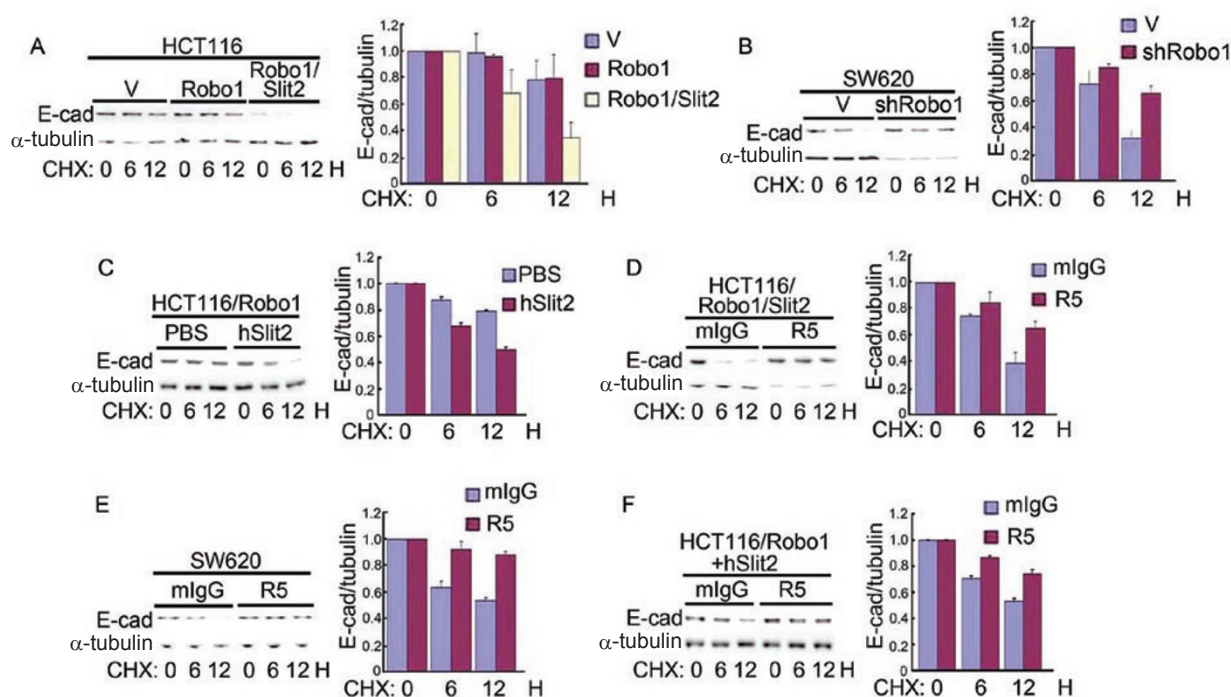


**Figure 6** Slit-Robo signaling degrades E-cad. (A-F) HCT116/V, HCT116/Robo1, HCT116/Robo1/Slit2, SW620/V and SW620/shRobo1 cells were treated with CHX, in the absence or presence of mlgG, R5, PBS and hSlit2, for a period of time as indicated. Cell lysates were immunoblotted with the Abs to E-cad (left upper panels) and  $\alpha$ -tubulin (left lower panels) and a ratio of E-cad over  $\alpha$ -tubulin (right panels) was calculated. Results are representative of at least three independent experiments (left panels) or the mean $\pm$ S.D. of three independent experiments (right panels).

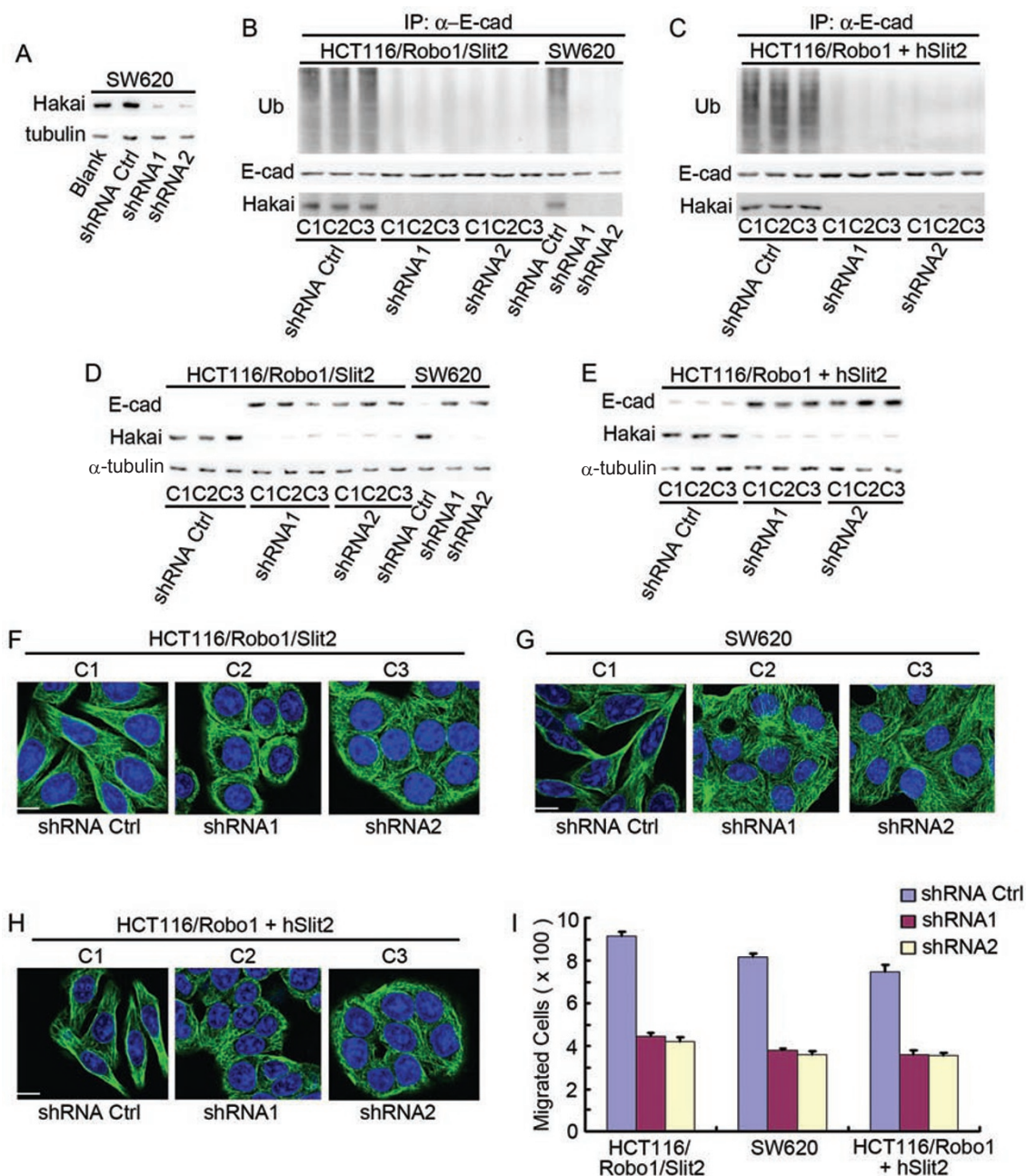


**Figure 7** Roles of Hakai in E-cad ubiquitination/degradation and EMT. **(A)** Identification of Hakai shRNAs. SW620 cells were either not transfected (blank) or transfected with the plasmids of shRNA control and shRNA1 and 2 of Hakai. Transfectants were immunoblotted for Hakai and  $\alpha$ -tubulin. **(B, C)** Effects of Hakai knockdown on E-cad ubiquitination. HCT116/Robo1/Slit2 and SW620 cells **(B)** or hSlit2-treated HCT116/Robo1 cells **(C)** were transfected with the plasmids of shRNA control and shRNA1 and 2 of Hakai followed by immunoblotting for ubiquitin (Ub, upper panels), E-cad (middle panels) and Hakai (lower panels). **(D, E)** Effects of Hakai knockdown on E-cad degradation. HCT116/Robo1/Slit2 and SW620 cells **(D)** or hSlit2-treated HCT116/Robo1 cells **(E)** were transfected with the plasmids of shRNA control and shRNA1 and 2 of Hakai followed by immunoblotting for E-cad (upper panels), Hakai (middle panels) and  $\alpha$ -tubulin (lower panels). **(F-H)** Effects of Hakai knockdown on cell morphology. HCT116/Robo1/Slit2 **(F)**, SW620 cells **(G)** or hSlit2-treated HCT116/Robo1 cells **(H)** were transfected with the plasmids of shRNA control and shRNA1 and 2 of Hakai followed by immunofluorescent staining as above. **(I)** Effects of Hakai knockdown on cell migration. HCT116/Robo1/Slit2, SW620 cells or hSlit2-treated HCT116/Robo1 cells were transfected with the plasmids of shRNA control and shRNA1 and 2 of Hakai followed by the Boyden chamber assay for determination of cell migration. Bars, 10  $\mu$ m. Results are representative of at least three independent experiments **(A-H)** or the mean $\pm$ S.D. of three independent experiments **(I)**.

naling may act as a common mechanism for induction of transformation in normal epithelial cells in addition to its role in colorectal epithelial cells. Of course, this provocative hypothesis awaits further validation.

*Expression of Slit2 and Robo1 correlates with enhanced metastasis and shortened survival*

To examine whether Slit2 and Robo1 expression correlates with tumor growth and metastasis of colorectal epithelial cells, we analyzed the expression of these proteins in human colorectal carcinoma tissue samples. We generated an IgG<sub>2a</sub> mAb to the N-terminal segment of human Slit2, S1, and an IgG<sub>1</sub> mAb to the C-terminal segment of rat Robo1, R4, as previously reported [16]. Here we examined the specificity of these mAbs. Lysates from HEK293 cells transfected with the plasmids of full-length human Slit1 to 3 or plain vector was immunoblotted with S1. S1 bound to full-length Slit2 (~200 kDa) and the N-terminal segment of Slit2 (~150 kDa), as well as to human Slit1 and 3 (Supplementary information, Figure S2C). In addition, HEK293 cells were transiently transfected with the plasmids of human Robo1 and 2 fused with the MYC tag and human Robo 3 and 4 fused with the FLAG tag. The 9E10 binding to the MYC tag detected Robo1 and 2 expression, whereas M2 binding to the FLAG tag detected Robo3 and 4 expression

(Supplementary information, Figure S2D). Interestingly, R4 bound to Robo1, but not to Robo2, 3 or 4. For negative controls, transfection of HEK293 cells with the plain vector resulted in no positive signals as measured by 9E10, M2 or R4. These results indicate that S1 is a pan-Slit mAb, specifically recognizing all three Slit proteins, whereas R4 is specific for human Robo1.

Using the S1 and R4 mAbs for pan-Slit and Robo1 immunofluorescent staining, we examined the tissue samples from 472 patients pathologically diagnosed with colorectal carcinoma (Figure 9A). Immunoreactivity for the pan-Slit antigens was seen in 17% more metastatic cancers than non-metastatic cancers while immunoreactivity for the Robo1 antigen was seen in 15% more metastatic cancers than non-metastatic cancers (Figure 9B). Interestingly, the frequency of both pan-Slit- and Robo1-positive staining in patients with metastatic cancer was 19% higher than that in non-metastatic cancer ( $P < 0.005$ ). To verify these immunological findings and to clarify which Slit constitutes the pan-Slit antigen, we extracted RNAs from the pan-Slit- and Robo1-positive and -negative tumor samples ( $n = 10$  for each group) and quantified Slit1-3 and Robo1-4 mRNAs by qRT-PCR. Compared with the pan-Slit and Robo1-negative tumor group, Slit2 and Robo1 were significantly upregulated in the pan-Slit- and Robo1-positive tumor group (Figure

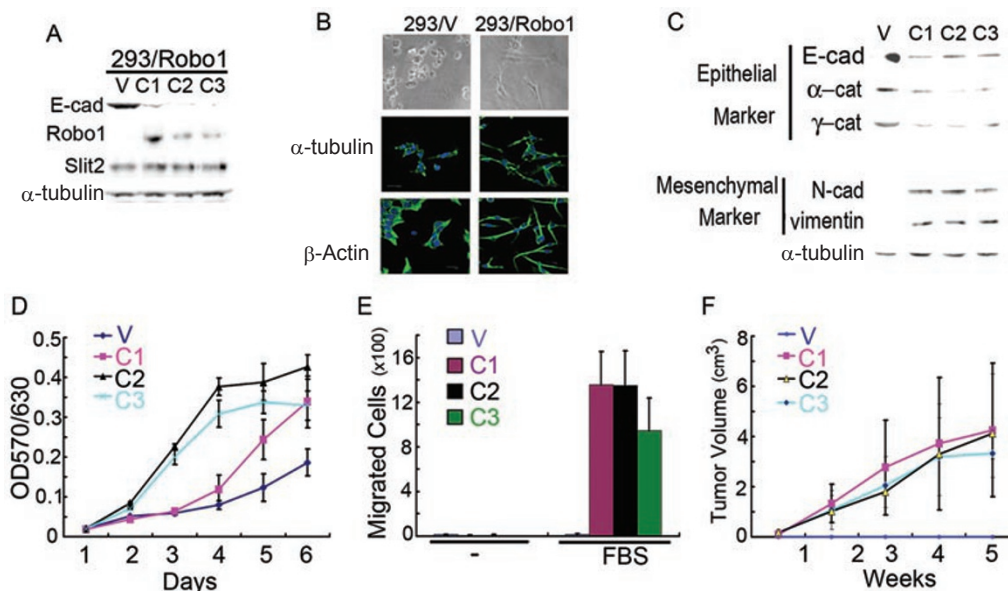


**Figure 8** Expression of Robo1 induces transformation of HEK293 cells. **(A)** HEK293 cells stably transfected with the plain vector (293/V) or the plasmid encoding Robo1 (293/Robo1). C1-3, clone 1-3. **(B)** Cell morphology of 293/V and 293/Robo1 cells (C1) with or without immunofluorescent staining of  $\alpha$ -tubulin and  $\beta$ -actin. Cell nuclei were stained with DAPI. Bars, 10  $\mu$ m. **(C)** Expression of epithelial and mesenchymal markers in 293/V and 293/Robo1 cells. **(D-F)** *In vitro* proliferation **(D)** and migration **(E)** and *in vivo* tumor formation **(F)**;  $n = 10$  for each group) of 293/V and 293/Robo1 cells. Results represent at least three independent experiments **(A-C)** or the mean  $\pm$  S.D. of three independent experiments **(D-F)**.

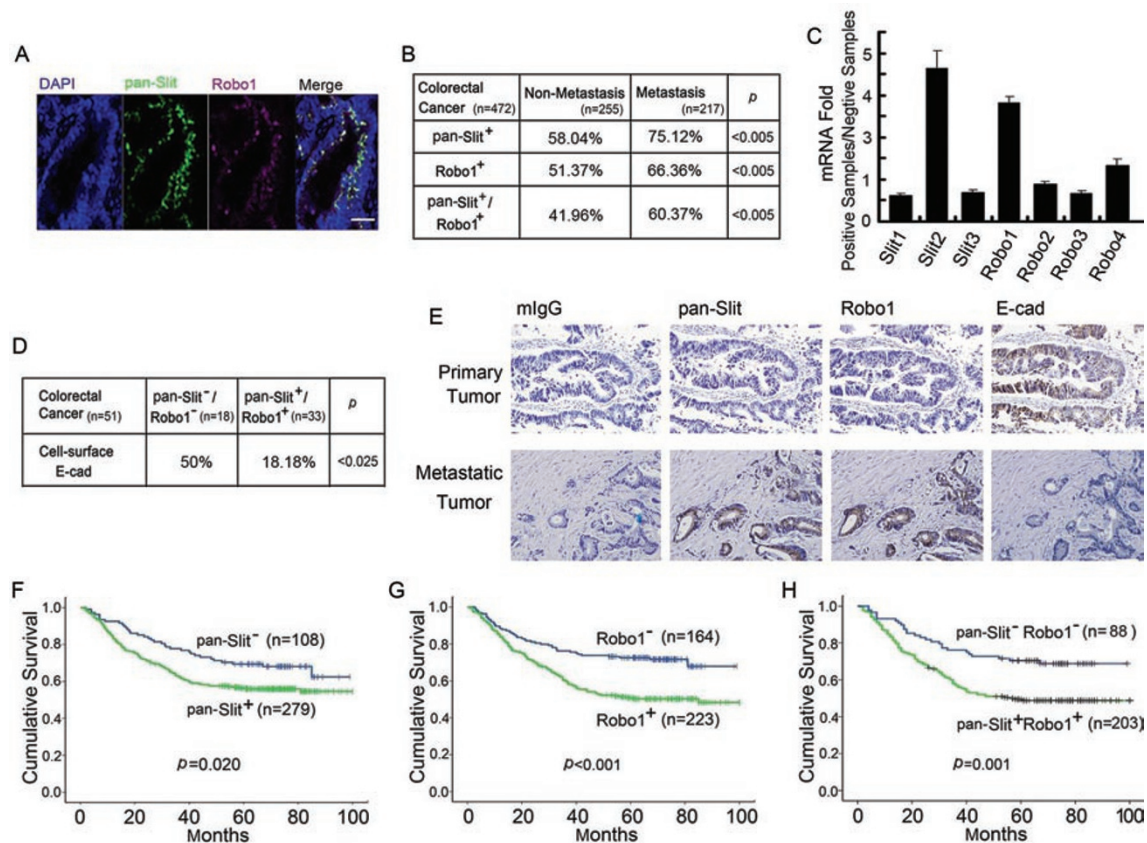


**Figure 9** Clinical significance of Slit-Robo expression in colorectal carcinoma. **(A)** Immunofluorescent staining of pan-Slit, Robo1 and nucleus (DAPI) and their co-localization in the colorectal carcinoma tissue specimen. Bars, 0.1 mM. **(B-D)** Expression of pan-Slit and Robo1 antigens **(B)** and Slit1-3 and Robo1-4 mRNAs **(C)** and their association with cell-surface E-cad **(D)** in the tissue specimen of non-metastatic and metastatic colorectal carcinoma. Pearson's  $\chi^2$ -test was used for statistical analysis **(B, D)**. **(E)** Immunohistochemical staining of pan-Slit, Robo1 and E-cad in continuous sections of primary (upper panels) and metastatic (lower panels) colorectal carcinoma. Results are representative of at least 10 independent experiments. Bars, 0.1 mM. **(F-H)** Long-term survival curves of colorectal carcinoma patients based on the immunoreactivity of pan-Slit **(F)**, Robo1 **(G)** and pan-Slit plus Robo1 **(H)**.

9C). These mRNA expression data thus confirmed our immunohistochemical results using the S1 and R4 mAbs. In addition, they demonstrated that Slit2, but not Slit1 or 3, was likely the major antigen detected by the S1 mAb. Notably, Robo4 mRNA was also slightly upregulated. Taken together, these findings indicate that the increased frequency of pan-Slit (mainly Slit2) and/or Robo1 expression may predict the metastasis or prognosis of colorectal carcinoma.

We next investigated whether pan-Slit and Robo1 expression was associated with the expression of E-cad in 51 cases of colorectal carcinoma (Figure 9D). As expected, the pan-Slit and Robo1 antigens negatively correlated with cell-surface E-cad. Using continuous tissue sectioning, we found that the epithelial layer of human colorectal primary tumors expressed cell-surface E-cad

when lacking pan-Slit antigen and Robo1 (Figure 9E, upper panel). In contrast, the tissue of colorectal metastatic tumors expressed pan-Slit antigen and Robo1 when losing E-cad expression (Figure 9E, lower panel). These findings in human samples suggest that Slit-Robo signaling may reversibly correlate to E-cad expression during the pathogenesis of tumor growth and metastasis.

We further evaluated whether the pan-Slit and Robo1 immunoreactivities correlated with overall survival in 387 patients with colorectal carcinoma. As suspected, we found that the pan-Slit antigen ( $P = 0.020$ ; Figure 9F), the Robo1 antigen ( $P < 0.001$ ; Figure 9G), and the pan-Slit plus Robo1 antigens ( $P = 0.001$ ; Figure 9H) all inversely correlated with overall survival, highlighting the clinical importance of Slit-Robo signaling in determining the prognosis of colorectal carcinoma.

## Discussion

This study demonstrates that engagement of Robo1 by Slit2 recruits Hakai to E-cad, culminating in E-cad ubiquitination and lysosomal degradation (Figure 10). Experimentally, ectopic expression of Slit2 and Robo1 and treatment of Robo1-positive cells with recombinant Slit2 induced an EMT-like phenotype, while knockdown of Robo1 or mAb blockade of Slit2 binding to Robo1 triggered a MET-like phenotype. Notably, our finding that expression of Robo1 triggers a malignant transformation in Slit2-positive HEK293 cells is fully consistent with the essential roles of Slit-Robo signaling during cell morphogenesis and organ development. Our findings, thus, have implications for the fundamental significance of Slit-Robo signaling in the malignant transformation of epithelial cells derived from different organs in addition to the colorectal intestine. Importantly, these experimental results are consistent with our clinical findings in 472 cases, in which metastatic human colorectal carcinoma tissue samples showed an increase in pan-Slit (mainly Slit2) and Robo1 expression compared to non-metastatic tissue samples. Remarkably, the pan-Slit and Robo1 immunoreactivities inversely correlated with overall survival in patients diagnosed with colorectal carcinoma, further underscoring the clinical significance of Slit-Robo signaling in the pathogenesis and prognosis of colorectal carcinoma.

During assembly of the *Drosophila* heart tube, two types of progenitor cells, cardioblasts and pericardial cells, are generated within bilateral fields in the lateral mesoderm. These cells align into rows and coordinately migrate, in an intricate manner, to the dorsal midline of the embryo, where they merge and assemble into a beating linear heart with a central lumen. Notably, cardioblasts are specifically adhered at dorsal and ventral attachment points in an E-cad-dependent manner, where

Slit and Robo transcripts are absent. In contrast, the apical surface of cardioblasts facing toward the lumen expresses Slit and Robo, where E-cad is absent. Overexpression of Slit and Robo thus results in ectopic lumen formation. However, Robo mutant embryo fails to form a cardiac tube between adherent contralateral cardioblasts due to aberrant expression of E-cad. It is thus apparent that Slit-Robo signaling inhibits E-cad-mediated cell adhesion, which is obligatory for lumen formation between apical cardioblasts [40-44]. In this context, our finding that the autocrine Slit-Robo interaction downregulates E-cad may plausibly explain the underlying molecular mechanism for the action of Slit-Robo signaling in cardiac cell polarity and tube lumen formation during development of *Drosophila* heart.

By promoter region CpG island hypermethylation and allele loss, *SLIT2* is reportedly inactivated in various cancer cell lines and primary lung, breast, intestinal, cervical and hepatocellular carcinomas, gliomas and lymphocytic leukemia, suggesting that *SLIT2* may act as a candidate tumor suppressor gene [45-51]. Notably, Slit2 is also found to enhance E-cad-mediated cell-cell adhesion of breast cancer MCF-7 cells [52] and to increase E-cad expression through downregulation of its transcriptional repressor, Snail, in lung cancer [53].

However, *SLIT2* promoter hypermethylation does not significantly associated with the clinical and pathological features of neuroblastoma, Wilms' tumor and renal cell carcinoma [54]. Hypermethylation of several CpG islands is frequently found in normal lung and breast tissues of cancer patients [55, 56]. Interestingly, the inhibitors of DNA methylation and histone deacetylases fail to reactivate *SLIT1-3*, *ROBO1* and *ROBO3* expression in cervical cancer, implicating a complex mechanism involved for the observed inactivation of these gene products [57]. Notably, in sharp contrast to the previous report [52], breast cancer MCF-7 cells are typically

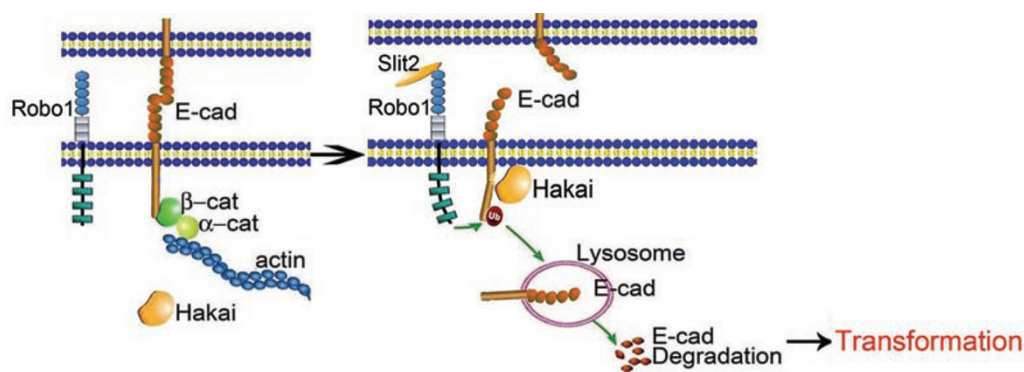


**Figure 10** Schematic illustration of our proposed model.

epithelial-like in morphology and express a high level of E-cad that is concentrated at the cell-cell contact [33, 58-61]. Furthermore, the engagement of Robo1 by Slit2 degrades N-cad and enhances motility of neuronal cells [62, 63]. The experimental findings of this study also provide compelling evidence for induction of EMT-like phenotype through downregulation of E-cad in colorectal epithelial cells by autocrine Slit-Robo signaling.

These seemingly paradoxical findings for the biological roles of Slit-Robo signaling in carcinogenesis are apparently reminiscent to the fascinating actions of these guidance cues in regulating both repulsive and attractive migration of such mammalian cells as neuronal, leukocytic, endothelial and cancerous cells [6, 64, 65], attesting to the context dependent and multifaceted roles of Slit-Robo signaling in cell migration and perhaps also in carcinogenesis. We speculate that in response to Slit2, it could be a combinatory array of intracellular signaling mechanisms downstream of cell-surface Robo1 that may not only regulate repulsive versus attractive cell migration, but also determine EMT-like versus MET-like phenotype of epithelial cells, governed by the temporal and spatial instruction and priming from neighboring cells at the given microenvironments. In this regard, Slit-Robo signaling may resemble TGF- $\beta$  [66], bone morphogenetic proteins [67], hepatic growth factor [68], Wnt/Frizzled [69, 70], estrogen [59] and microRNAs (miR-200 family and miR-205) [71] for reversible epithelial to mesenchymal-like transition and cell migration. Importantly, phenotypic plasticity of epithelial cells is obligatory for tube formation during development and for metastasis during carcinogenesis [23-26].

Intracellular molecules downstream of Robo signaling have emerged as key regulators for its biological functional activities on the targeting cells. Robo utilizes a variety of different signaling components in different cell types, such as Mena/Ab1 [5, 72], Slit-Robo GTPase-activating protein 1 [73] and phosphoinositol-3 kinase [16]. In this context, it should be mentioned that no tyrosine phosphorylation of immunoprecipitated Robo1 was detected in the lysates of HCT116/Robo1/Slit2 or SW620 cells (data not shown) and no c-Abl binding to Robo1 [62, 63] was found in SW620 cells (data not shown). These results apparently suggest that the downstream components of Slit-Robo signaling may be overlapping but distinct between colorectal epithelial cells and neuronal/retinal cells.

Previous studies by us and others have shown that Slit-Robo signaling critically participates in vasculogenesis, angiogenesis and lymphangiogenesis [16-22, 74-78]. For instance, a variety of cancer cells secrete Slit2, which binds to Robo1 expressed on vascular endothelial cells

and mediates tumor angiogenesis via a paracrine mechanism [16-19, 21]. In addition, we have recently demonstrated that Slit2 binds to Robo1 expressed on lymphatic endothelial cells, which induces lymphangiogenesis and lymphatic metastasis [22]. This study demonstrates the existence of an autocrine mechanism for mediating tumor cell-tumor cell signaling during growth and metastasis of colorectal carcinoma. On the basis of these observations, we propose that Slit-Robo signaling may act through both paracrine and autocrine mechanisms to synergistically promote the malignant transformation of colorectal epithelial cells. In this context, the profoundly potent effects of R5, which blocks the Slit2-Robo1 interaction, on *in vivo* tumor growth and liver metastasis of HCT116/Robo1/Slit2 cells and SW620 cells can be partially explained by its inhibition of paracrine tumor angiogenesis mediated by Slit-Robo signaling. Although R5 markedly inhibited *in vitro* growth of HCT116/Robo1/Slit2 cells and SW620 cells in the present study, it did not inhibit human malignant melanoma A375 cells in a previous study (see Figure 3I of reference [16]). Overexpression of Slit2 did not promote A375 cell growth in culture (see Supplementary information, Figure S1B of reference [16]). These seemingly contradictory results are because of the lack of detectable Robo1 expression in A375 cells and the absence of the autocrine Slit-Robo interaction (see Figure 1H of reference [16]). Therefore, it is reasonable to conclude that blockade of Slit-Robo signaling may potentially inhibit tumor angiogenesis and effectively prevent malignant transformation for suppression of tumor growth and metastasis in colorectal carcinoma. As a result, we believe that inhibitors of Slit-Robo signaling warrant clinical testing for treating colorectal carcinoma.

## Material and Methods

### *Plasmids, antibodies and chemicals*

Monoclonal Abs specific for human Robo1, Slit2, pan-Slit as well as R5 and its isotype-matched mouse IgG<sub>2b</sub> control were prepared and characterized as previously described [16]. The plasmid of snail (16218) was purchased from Addgene; human Slit1 (KIAA0813) and Slit3 (KIAA0814) were obtained from KAZUSA DNA Research Institute; human Robo2-4 were purchased from OriGene. The control shRNA (RHS4430-98524293) and shRNA1 and 2 (RHS4430-98714486 and RHS4430-98841956) of Hakai were purchased from Open Biosystems. Primary mAbs to E-cad,  $\alpha$ -cat,  $\beta$ -cat,  $\gamma$ -cat and N-cad were obtained from BD Biosciences. Monoclonal Abs to vimentin,  $\alpha$ -tubulin,  $\beta$ -actin, CHX, chloroquin and MG132 were purchased from Sigma. Hakai, ubiquitin and LAMP-1 Abs were purchased from Santa Cruz Biotechnology. The second anti-Hakai Ab (ab91185) was purchased from Abcam.

### *Cell cultures, stable cell lines and treatment*

Human colorectal carcinoma cell lines SW620 (CCL-227),



### Colony formation assay

For determination of cell transformation, a bottom layer of 0.6% agar noble in DMEM without serum was first placed onto a six-well plate. Cells were seeded in 0.3% top agar noble in DMEM with 10% FBS. Fresh top agar was added after 10 days. Colonies that had formed were counted after 3 weeks.

### Xenograft model of tumor growth and metastasis

Cells were resuspended at  $1 \times 10^7$  cells/ml and an aliquot of 0.1 ml cell suspension was injected subcutaneously into athymic nude mice [16]. For antibody inhibition experiments, mice bearing HCT116/Robo1/Slit2 or SW620 cell tumors were treated with intraperitoneal injections of R5 or mIgG<sub>2b</sub> control twice per week (1 mg per injection). For metastasis measurements, mouse livers and lungs were collected after subcutaneous inoculation of cells for 5 weeks followed by counting of tumor nodules (routinely more than five nodules per liver or lung).

### Immunohistochemical staining

Patient tissue samples of colorectal carcinoma along with the corresponding clinical follow-up details were collected from the Department of Pathology, Nanfang Hospital over a period of more than 10 years. For determination of pan-Slit and Robo1 immunoreactivity [16], cytosolic staining of yellowish or brownish granules was graded as follows: 0 for background staining, 1 for faint staining, 2 for moderate staining and 3 for strong staining. In addition, positive staining areas in entire tissue section were graded as follows: 0 for < 10%, 1 for 11-25%, 2 for 26-50% and 3 for 51-100%. When combining these two parameters, 0-2 and  $\geq 3$  were defined as negative and positive for antigen, respectively.

### Statistical analysis

The difference in frequency between patients with and without metastasis was evaluated using  $\chi^2$ -test. To compute correlation coefficients of immunostaining scores between two proteins, Spearman's rank correlation coefficient was used. Overall survival was represented in months, which was defined as the interval between the date of the surgery and the date of death or last follow-up. Overall survival curves were estimated by the Kaplan-Meier method, and the difference in survival was evaluated using the log-rank test. The *P*-values of < 0.05 and 0.01 were considered statistically significant and very significant. All computations were made with R 2.9.0 (<http://www.r-project.org>).

### Acknowledgments

We thank Biao Wang for preliminary studies and Michael J Franklin for editing the manuscript. We are grateful to Elaine Fuchs for the plasmid of the E-cadherin promoter luciferase reporter. This work was supported by grants from the Ministry of Science and Technology of China (2010CB529702 to XY and L-JW, 2010CB529403 to Y-QD), National Science Foundation of China (30871304 to L-JW) and National Institutes of Health (CA126897, AI064743 to J-GG).

### References

- Kidd T, Brose K, Mitchell KJ, *et al.* Roundabout controls axon crossing of the CNS midline and defines a novel sub-family of evolutionarily conserved guidance receptors. *Cell* 1998; **92**:205-215.
- Brose K, Bland KS, Wang KH, *et al.* Slit proteins bind Robo receptors and have an evolutionarily conserved role in repulsive axon guidance. *Cell* 1999; **96**:795-806.
- Li HS, Chen JH, Wu W, *et al.* Vertebrate Slit, a secreted ligand for the transmembrane protein Roundabout, is a repellent for olfactory bulb axons. *Cell* 1999; **96**:807-818.
- Plump AS, Erskine L, Sabatier C, *et al.* Slit1 and Slit2 cooperate to prevent premature midline crossing of retinal axons in the mouse visual system. *Neuron* 2002; **33**:219-232.
- Bashaw GJ, Kidd T, Murray D, Pawson T, Goodman CS. Repulsive axon guidance: Abelson and Enabled play opposing roles downstream of the roundabout receptor. *Cell* 2000; **101**:703-715.
- Dickson BJ, Gilestro GF. Regulation of commissural axon path finding by Slit and its Robo receptors. *Annu Rev Cell Dev Biol* 2006; **22**:651-675.
- Wu JY, Feng LL, Park HT, *et al.* The neuronal repellent Slit inhibits leukocyte chemotaxis induced by chemotactic factors. *Nature* 2001; **410**:948-952.
- Guan H, Zu G, Xie Y, *et al.* Neuronal repellent Slit2 inhibits dendritic cell migration and the development of immune responses. *J Immunol* 2003; **171**:6519-26.
- Kanellis J, Garcia GE, Li P, *et al.* Modulation of inflammation by Slit protein *in vivo* in experimental crescentic glomerulonephritis. *Am J Pathol* 2004; **165**:341-352.
- Prasad A, Qamri Z, Wu J, Ganju RK. Slit2/Robo1 modulates the CXCL12/CXCR4-induced chemotaxis of T cells. *J Leukoc Biol* 2007; **82**:465-476.
- Altay T, McLaughlin B, Wu JY, Park TS, Gidday JM. Slit modulates cerebrovascular inflammation and mediates neuroprotection against global cerebral ischemia. *Exp Neurol* 2007; **207**:186-194.
- Tole S, Mukovozov IM, Huang YW, *et al.* The axonal repellent, Slit2, inhibits directional migration of circulating neutrophils. *J Leukoc Biol* 2009; **86**:1403-1415.
- Schmid BC, Reznicek G.A, Fabjani G, Yoneda T, Leodolter S, Zeillinger R. The neuronal guidance cue Slit2 induces targeted migration and may play a role in brain metastasis of breast cancer cells. *Breast Cancer Res Treat* 2007; **106**:333-342.
- Mertsch S, Schmitz N, Jeibmann A, Geng JG, Paulus W, Senner V. Slit2 involvement in glioma cell migration is mediated by Robo1 receptor. *J Neurooncol* 2008; **87**:1-7.
- Yuasa-Kawada J, Kinoshita-Kawada M, Rao Y, Wu JY. Deubiquitinating enzyme USP33/VDU1 is required for Slit signaling in inhibiting breast cancer cell migration. *Proc Natl Acad Sci USA* 2009; **106**:14530-14535.
- Wang B, Xiao Y, Ding, B, *et al.* Induction of tumor angiogenesis by Slit-Robo signaling and inhibition of cancer growth by blocking Robo activity. *Cancer Cell* 2003; **4**:19-29.
- Wang LJ, Zhao Y, Han B, *et al.* Targeting Slit-Roundabout signaling inhibits tumor angiogenesis in chemical-induced squamous cell carcinogenesis. *Cancer Sci* 2008; **99**:510-517.
- Urbich C, Rössig L, Kaluza D, *et al.* HDAC5 is a repressor of angiogenesis and determines the angiogenic gene expression pattern of endothelial cells. *Blood* 2009; **113**:5669-5679.
- Shen F, Liu X, Geng JG, Guo SW. Increased immunoreac-

- tivity to Slit/Robo1 in ovarian endometriomas. *Am J Pathol* 2009; **175**:479-488.
- 20 Zhang B, Dietrich UM, Geng JG, Bicknell R, Esko JD, Wang L. Repulsive axon guidance molecule Slit3 is a novel angiogenic factor. *Blood* 2009; **114**:4300-4309.
- 21 Ma S, Liu X, Geng JG, Guo SW. Increased SLIT immunoreactivity as a biomarker for recurrence in endometrial carcinoma. *Am J Obstet Gynecol* 2010; **202**:68.e1-68.e11.
- 22 Yang XM, Han HX, Sui F, Dai YM, Chen M, Geng JG. Slit-Robo signaling mediates lymphangiogenesis and promotes tumor lymphatic metastasis. *Biochem Biophys Res Commun* 2010; **396**:571-577.
- 23 Grunert S, Jechlinger M, Beug H. Diverse cellular and molecular mechanism contribute to epithelial plasticity and metastasis. *Nat Rev Mol Cell Biol* 2003; **4**:657-665.
- 24 Gumbiner BM. Regulation of cadherin-mediated adhesion in morphogenesis. *Nat Rev Mol Cell Biol* 2005; **6**:622-634.
- 25 Radisky DC. Epithelial-mesenchymal transition. *J Cell Sci* 2005; **118**:4325-4326.
- 26 Thiery JP, Sleeman JP. Complex networks orchestrate epithelial-mesenchymal transitions. *Nat Rev Mol Cell Biol* 2006; **7**:131-142.
- 27 Pokutta S, Weis WI. Structure and mechanism of cadherin and catenins in cell-cell contacts. *Annu Rev Cell Dev Biol* 2007; **23**:237-261.
- 28 Maina F, Pante G, Helmbacher F, *et al.* Coupling Met to specific pathways results in distinct developmental outcomes. *Mol Cell* 2001; **7**:1293-1306.
- 29 Lu Z, Ghosh S, Wang Z, Hunter T. Downregulation of caveolin-1 function by EGF leads to the loss of E-cadherin, increased transcriptional activity of  $\beta$ -catenin, and enhanced tumor cell invasion. *Cancer Cell* 2003; **4**:499-515.
- 30 Shimizu Y, Yamamichi N, Saitoh K, *et al.* Kinetics of v-src-induced epithelial-mesenchymal transition in developing glandular stomach. *Oncogene* 2003; **22**:884-893.
- 31 Palacios F, Tushir JS, Fujita Y, D'Souza-Schorey C. Lysosomal targeting of E-cadherin: a unique mechanism for the downregulation cell-cell adhesion during epithelial to mesenchymal transitions. *Mol Cell Biol* 2005; **25**:389-402.
- 32 Janda E, Nevolo M, Lehmann K, Downward J, Beng H, Grieco M. Raf plus TGF- $\beta$ -dependent EMT is initiated by endocytosis and lysosomal degradation of E-cadherin. *Oncogene* 2006; **25**:7117-7130.
- 33 Bryant DM, Kerr MC, Hammond LA, *et al.* EGF induces macropinocytosis and SNX1-modulated recycling of E-cadherin. *J Cell Sci* 2007; **120**:1818-1828.
- 34 Wheelock MJ, Shintani Y, Maeda M, Fukumoto Y, Johnson KR. Cadherin switching. *J Cell Sci* 2008; **121**:727-735.
- 35 Shen Y, Hirsch DS, Sasiela CA, Wu WJ. Cdc42 regulates E-cadherin ubiquitination and degradation through an epidermal growth factor receptor to Src-mediated pathway. *J Biol Chem* 2008; **283**:5127-5137.
- 36 Kobiela A, Fuchs E.  $\alpha$ -catenin: at the junction of intercellular adhesion and actin dynamics. *Nat Rev Mol Cell Biol* 2004; **5**:614-625.
- 37 Gröne J, Doebler O, Loddenkemper C, Hotz B, Buhr HJ, Bhargava S. Robo1/Robo4: differential expression of angiogenic markers in colorectal cancer. *Oncol Rep* 2006; **15**:1437-1443.
- 38 Labbe E, Lock L, Letamendia A, *et al.* Transcriptional cooperation between the transforming growth factor and Wnt pathways in mammary and Intestinal tumorigenesis. *Cancer Res* 2007; **67**:75-84.
- 39 Fujita Y, Krause G, Scheffner M, *et al.* Hakai, a c-Cbl-like protein, ubiquitinates and induces endocytosis of the E-cadherin complex. *Nat Cell Biol* 2002; **4**:222-231.
- 40 Qian L, Liu J, Bodmer R. Slit and Robo control cardiac cell polarity and morphogenesis. *Curr Biol* 2005; **15**:2271-2278.
- 41 MacMullin A, Jacobs JR. Slit coordinates cardiac morphogenesis in *Drosophila*. *Dev Biol* 2006; **293**:154-164.
- 42 Santiago-Martinez E, Soplop NH, Kramer SG. Lateral positioning at the dorsal midline: Slit and Roundabout receptors guide *Drosophila* heart cell migration. *Proc Natl Acad Sci USA* 2006; **103**:12441-12446.
- 43 Santiago-Martinez E, Soplop N.H, Kramer SG. Repulsion by Slit and Roundabout prevents Shotgun/E-cadherin-mediated cell adhesion during *Drosophila* heart tube lumen formation. *J Cell Biol* 2008; **182**:241-248.
- 44 Medioni C, Astier M, Zmojdian M, Jagla K, Semeriva M. Genetic control of cell morphogenesis during *Drosophila melanogaster* cardiac tube formation. *J Cell Biol* 2008; **182**:249-261.
- 45 Dallol A, Da Silva NF, Viacava P, *et al.* SLIT2, a human homolog of the *Drosophila* Slit2 gene, has tumor suppressor activity and is frequently inactivated in lung and breast cancers. *Cancer Res* 2002; **62**:5874-5880.
- 46 Dallol A, Krex D, Hesson L, Eng C, Maher ER, Latif F. Frequent epigenetic inactivation of the *SLIT2* gene in gliomas. *Oncogene* 2003; **22**:4611-4616.
- 47 Dallol A, Morton D, Maher ER, Latif F. *SLIT2* axon guidance molecule is frequently inactivated in colorectal cancer and suppresses growth of colorectal carcinoma cells. *Cancer Res* 2003; **63**:1054-1058.
- 48 Sharma G, Mirza S, Prasad CP, Srivastava A, Gupta SD, Ralhan R. Promoter hypermethylation of p16INK4A, p14ARF, cyclin D2 and Slit2 in serum and tumor DNA from breast cancer patients. *Life Sci* 2007; **80**:1873-1881.
- 49 Singh RK, Indra D, Mitra S, *et al.* Deletions in chromosome 4 differentially associated with the development of cervical cancer: evidence of Slit2 as a candidate tumor suppressor gene. *Hum Genet* 2007; **122**:71-81.
- 50 Dunwell TL, Dickinson RE, Stankovic T, *et al.* Frequent epigenetic inactivation of the *SLIT2* gene in chronic and acute lymphocytic leukemia. *Epigenetics* 2009; **4**:265-269.
- 51 Jin J, You H, Yu B, *et al.* Epigenetic inactivation of *SLIT2* in human hepatocellular carcinomas. *Biochem Biophys Res Commun* 2009; **379**:86-91.
- 52 Prasad A, Paruchuri V, Preet A, Latif F, Ganju RK. Slit-2 induces a tumor-suppressive effect by regulating beta-catenin in breast cancer cells. *J Biol Chem* 2008; **283**:26624-26633.
- 53 Tseng RC, Lee SH, Hsu HS, *et al.* *SLIT2* attenuation during lung cancer progression deregulates beta-catenin and E-cadherin and associates with poor prognosis. *Cancer Res* 2010; **70**:543-551.
- 54 Astuti D, Da Silva NF, Dallol A, *et al.* *SLIT2* promoter methylation analysis in neuroblastoma, Wilms' tumour and renal cell carcinoma. *Br J Cancer* 2004; **90**:515-521.
- 55 Dammann R, Strunnikova M, Schagdarsurengin U, *et al.* CpG

- island methylation and expression of tumour-associated genes in lung carcinoma. *Eur J Cancer* 2005; **41**:1223-1236.
- 56 Dietrich D, Lesche R, Tetzner R, *et al.* Analysis of DNA methylation of multiple genes in microdissected cells from formalin-fixed and paraffin-embedded tissues. *J Histochem Cytochem* 2009; **57**:477-489.
- 57 Narayan G, Goparaju C, Arias-Pulido H, *et al.* Promoter hypermethylation-mediated inactivation of multiple Slit-Robo pathway genes in cervical cancer progression. *Mol Cancer* 2006; **5**:16-25.
- 58 Li L, Backer J, Wong AS, Schwanke EL, Stewart BG, Pasdar M. Bcl-2 expression decreases cadherin-mediated cell-cell adhesion. *J Cell Sci* 2003; **116**:3687-3700.
- 59 Planas-Silva MD, Waltz PK. Estrogen promotes reversible epithelial-to-mesenchymal-like transition and collective motility in MCF-7 breast cancer cells. *J Steroid Biochem Mol Biol* 2007; **104**:11-21.
- 60 Laffin B, Wellberg E, Kwak HI, *et al.* Loss of single-minded-2s in the mouse mammary gland induces an epithelial-mesenchymal transition associated with up-regulation of slug and matrix metalloproteinase 2. *Mol Cell Biol* 2007; **28**:1936-1946.
- 61 Arima Y, Inoue Y, Shibata T, *et al.* Rb depletion results in deregulation of E-cadherin and induction of cellular phenotypic changes that are characteristic of the epithelial-to-mesenchymal transition. *Cancer Res* 2008; **68**:5104-5112.
- 62 Rhee J, Mahfooz NS, Arregui C, Lilien J, Balsamo J, VanBerkum MF. Activation of the repulsive receptor Roundabout inhibits N-cadherin mediated cell adhesion. *Nat Cell Biol* 2002; **4**:798-805.
- 63 Rhee J, Buchan T, Zukerberg L, Lilien J, Balsamo J. Cables links Robo-bound Abl kinase to N-cadherin bound  $\beta$ -catenin to mediate Slit-induced modulation of adhesion and transcription. *Nat Cell Biol* 2007 **9**:883-892.
- 64 Wong K, Park HT, Wu JY, Rao Y. Slit proteins: molecular guidance cues for cells ranging from neurons to leukocytes. *Curr Opin Genet Dev* 2002; **12**:583-591.
- 65 Wang B, Geng JG. Highly-conserved mechanisms of cell migration and contact in immune and nervous systems. *Med Hypotheses Res* 2005; **2**:315-323.
- 66 Heldin CH, Lanström M, Moustakas A. Mechanism of TGF- $\beta$  signaling to growth arrest, apoptosis, and epithelial-mesenchymal transition. *Curr Opin Cell Biol* 2009; **21**:166-176.
- 67 Gressner OA, Rizk MS, Kovalenko E, Weiskirchen R, Gressner AM. Changing the pathogenetic roadmap of liver fibrosis? Where did it start; where will it go? *J Gastroenterol Hepatol* 2008; **23**:1024-1035.
- 68 Battaglia S, Benzoubir N, Nobilet S, *et al.* Liver cancer-derived hepatitis C virus core proteins shift TGF-beta responses from tumor suppression to epithelial-mesenchymal transition. *PLoS One* 2009; **4**:e4355.
- 69 Gregorieff A, Clevers H. Wnt signaling in the intestinal epithelium: from endoderm to cancer. *Genes Dev* 2005; **19**:877-890.
- 70 Heuberger J, Birchmeier W. Interplay of cadherin-mediated cell adhesion and canonical Wnt signaling. *Cold Spring Harb Perspect Biol* 2010; **2**:a002915.
- 71 Gregory PA, Bracken CP, Goodall GJ. MicroRNAs as regulators of epithelial-mesenchymal transition. *Cell Cycle* 2008; **7**:3112-3118.
- 72 Fritz JL, VanBerkum MF. Calmodulin and Son of sevenless dependent signaling pathways regulate midline crossing of axon in the *Drosophila* CNS. *Development* 2000; **127**:1991-2000.
- 73 Wong K, Ren XR, Huang YZ, *et al.* Signal transduction in neuronal migration: roles of GTPase activating proteins and the small GTPase cdc42 in the Slit-Robo pathway. *Cell* 2001; **107**:209-221.
- 74 Huminiecki L, Gorn M, Suchting S, Poulosom R, Bicknell R. Magic roundabout is a new member of the roundabout receptor family that is endothelial specific and expressed at sites of active angiogenesis. *Genomics* 2002; **79**:547-552.
- 75 Bedell VM, Yeo SY, Park KW, *et al.* Roundabout4 is essential for angiogenesis *in vivo*. *Proc Natl Acad Sci USA* 2005; **102**:6373-6378.
- 76 Jones CA, London NR, Chen H, *et al.* Robo4 stabilizes the vascular network by inhibiting pathologic angiogenesis and endothelial hyperpermeability. *Nat Med* 2008; **14**:448-453.
- 77 Sheldon H, Andre M, Legg JA, *et al.* Active involvement of Robo1 and Robo4 in filopodia formation and endothelial cell motility mediated via WASP and other actin nucleation-promoting factors. *FASEB J* 2009; **23**:513-522.
- 78 Jones CA, Nishiya N, London NR, *et al.* Slit2-Robo4 signaling promotes vascular stability by blocking Arf6 activity. *Nat Cell Biol* 2009; **11**:1325-1331.
- 79 Wang HB, Wang JT, Zhang L, *et al.* P-selectin primes leukocyte integrin activation during inflammation. *Nat Immunol* 2007; **8**:882-892.
- 80 Xia YF, Ye BQ, Li YD, *et al.* Andrographolide attenuates inflammation by inhibition of NF-kappa B activation through covalent modification of reduced cysteine62 of p50. *J Immunol* 2004; **173**:4207-4217.

(Supplementary information is linked to the online version of the paper on the *Cell Research* website.)